RSC Advances

PAPER

View Article Online
View Journal | View Issue

Cite this: *RSC Adv.*, 2025, **15**, 42887

Investigation on the membrane fouling control and mechanism induced by IOM using heat-activated peroxydisulfate pre-oxidation

Weiwei Huang,[ab] Yuning Zhang,[ab] Weiwei Lv,[ab] Hang Yang,[ab] Quan Yuan[ab] and Wenzong Zhou*[ab]

Membrane fouling induced by intracellular organic matter (IOM) presents a major challenge in the ultrafiltration (UF) of algal-laden water. While extracellular organic matter (EOM) has been widely studied, the role of IOM and its control mechanism remain insufficiently understood. This study systematically investigated the mitigation of IOM-induced UF membrane fouling through heat-activated peroxymonosulfate (PMS) pre-oxidation. The effects of varying PMS dosages (0.2–0.8 mM) on fouling behavior and mechanisms were thoroughly evaluated. The results demonstrated that the IOM released by *Chlorella* caused severe membrane fouling during UF. Membrane fouling was significantly mitigated after heat-activated PMS pretreatment when the dosage exceeded 0.2 mM, with the optimal performance obtained at the PMS dosage of 0.6 mM. PMS pretreatment effectively removed macro and medium molecular organics in IOM that were primarily responsible for membrane fouling. Moreover, PMS pretreatment influenced the surface morphology and hydrophobicity of the fouling layer. The interaction energy between the membrane and foulants was also changed. The fouling mechanism exhibited a shift in the dominant mode, while the untreated IOM primarily caused cake layer formation, and PMS pre-oxidation altered the fouling behavior toward pore blocking. Collectively, this research proposed a practical strategy to mitigate membrane fouling induced by IOM in the UF of algal-laden water.

Received 10th July 2025
Accepted 7th October 2025

DOI: 10.1039/d5ra04924e

rsc.li/rsc-advances

1 Introduction

Water is an essential natural resource for human survival and socio-economic development. However, over the past few decades, the increasing discharge of industrial and domestic wastewater, coupled with the impacts of global warming, has led to the gradual deterioration of water quality and the widespread occurrence of eutrophication. One of the most concerning consequences of eutrophication is algal bloom, which has attracted considerable attention due to the release of various secondary metabolites, including high concentrations of algal toxins and odorous compounds during bloom events.[1] These phenomena can severely impair water treatment processes by increasing the coagulant demand, accelerating the membrane fouling in downstream filtration units, and raising the frequency of backwashing. Ultrafiltration (UF) has been recognized as an effective technology for removing harmful algae owing to its superior ability to physically retain algal cells compared with conventional treatment methods. Numerous studies have investigated the performance of UF for algal removal.[2,3] However, membrane fouling continues to be a critical challenge hindering the large-scale adoption of UF, mainly attributed to the discharge of algogenic organic matter (AOM) that significantly increases the operational costs and reduces the membrane lifespan. Previous studies have demonstrated that the reversible and irreversible fouling induced by algae are complex processes, which are affected not only by the intact algal cells but also by the extracellular organic matter (EOM) and intracellular organic matter (IOM) secreted.[4,5]

To address membrane fouling during the UF process, various pretreatment strategies, including pre-coagulation, pre-filtration, and pre-oxidation, have been proposed.[6,7] Advanced oxidation processes (AOPs) have emerged as effective pretreatment techniques for mitigating membrane fouling.[8,9] In particular, persulfate (PS)-based AOPs, such as peroxymonosulfate (PMS, HSO_5^-) and peroxydisulfate (PDS, $S_2O_8^{2-}$), have garnered increasing attention in recent years due to their higher oxidative potential for removing micro-pollutants and ability to control membrane fouling than other pretreatments.[9,10] Compared with traditional oxidants, PMS and PDS offer several advantages, such as they are easy to store and transport (as they are solid-phase oxidants), environmentally benign, and chemically stable with wide pH tolerance. Sulfate radicals ($SO_4^{\bullet-}$) generated from PS

[a]*Laboratory of Integrated Rice-Fish Farming Ecosystem, Ministry of Agriculture and Rural Affairs, Eco-Environmental Protection Research Institute, Shanghai Academy of Agricultural Sciences, Shanghai 201403, China. E-mail: zhouwz001@163.com; Tel: +86 21 65982691*

[b]*Shanghai Engineering Research Centre of Low-carbon Agriculture, Shanghai 201403, China*

activation also exhibit superior oxidative properties compared to hydroxyl radicals (˙OH) derived from H_2O_2 activation, including a greater redox potential (2.5–3.1 V *vs.* 1.8–2.7 V), a notably extended half-life (30–40 μs *vs.* <1 μs), and lower second-order rate constants with various pollutants (2.5–8.1 × 10^7 M^{-1} s^{-1} *vs.* 1.6–3.3 × 10^8 M^{-1} s^{-1}).[11] Many studies have explored the efficacy of PS-based AOPs in algae-laden water treatment. Wan *et al.* compared UV/PS, UV/chlorine, and UV/H_2O_2 pretreatments and found that UV/PS achieved superior performance in alleviating membrane fouling.[12] Liu *et al.* suggested that Fe(II)/PS pretreatment was effective in reducing membrane fouling and improving the removal efficiency of algal contaminants.[13] Similarly, it was found that the UV/Fe(II)/PMS pretreatment markedly improved ultrafiltration performance during algal-laden wastewater treatment.[14] Despite these promising results, since the application of PMS and PDS for algal-laden water treatment and membrane fouling control remains relatively limited,[15,16] and a variety of approaches have been employed to activate persulfates, such as nano-carbon materials, carbon-based catalysts, zero-valent iron, ferrous ions, transition metals, and ultraviolet (UV) irradiation,[17,18] a comprehensive study of their effectiveness in removing organic substances and alleviating membrane fouling is lacking and warrants further investigation.

Heat activation has attracted considerable interest owing to its distinctive benefits, especially the enhancement of reaction efficiency achieved at elevated temperatures.[19] Furthermore, heat-activated advanced oxidation processes offer a sustainable treatment approach by utilizing industrial waste heat to drive pollutant degradation, thereby reducing reliance on additional chemical inputs.[20,21] Numerous studies have successfully applied thermally activated PS for the treatment of wastewater and natural surface waters, demonstrating promising results in contaminant removal.[22] Regarding algae-laden water treatment, although some research has explored the removal of *Microcystis aeruginosa* and membrane fouling in membrane distillation systems,[23] the algal-laden water contains not only intact algal cells but also EOM and IOM, all of which contribute significantly to membrane fouling. Therefore, a more comprehensive evaluation of the performance of heat-activated PS in UF systems treating algae-laden water is still urgently needed to fully understand its effectiveness in mitigating fouling caused by these diverse organic fractions.

IOM is primarily released through cell autolysis during the algal late growth stages or under external stress conditions, such as oxidative stress and hydraulic shear.[24–26] Previous studies have shown that IOM present in membrane-driven water purification procedures can markedly promote the generation of disinfection byproducts (DBPs), which are also associated with taste and odor issues.[27,28] Moreover, in comparison with EOM, IOM has a more detrimental effect on UF performance, causing greater flux decline and more severe irreversible membrane fouling. This is primarily owing to the accumulation of tighter and thicker cake layers on the membrane surface.[29,30] Although substantial research efforts have been directed toward mitigating membrane fouling attributed to EOM,[31,32] the mitigation of fouling induced by IOM has received comparatively limited attention. Given its profound implications for membrane performance and water quality, there is an urgent need for more comprehensive investigations into effective control strategies for IOM-induced membrane fouling. However, according to available information, the role of PMS pretreatment in modulating IOM-induced membrane fouling during algal-laden water treatment remains poorly understood, which needs to be clearly established.

This research thus aims to investigate the effectiveness of heat-activated PMS pretreatment in mitigating membrane fouling caused by IOM, with the objectives: (1) to analyze the removal of organics by various PMS treatments; (2) to assess the effectiveness of heat-activated PMS in controlling the IOM-induced membrane fouling; and (3) to clarify the underlying fouling control mechanisms associated with IOM, following PMS pre-oxidation. This study is expected to provide practical and effective contributions to the control of membrane fouling in algae-laden water treatment, with particular emphasis on algal late growth stages.

2 Materials and methods

2.1 Algae cultivation and IOM extraction

Chlorella was obtained from the Institute of Aquatic Biology, Chinese Academy of Sciences, and cultured in BG-11 medium under an irradiance of approximately 90 μmol m^{-2} s^{-1} at 25 °C, with a photoperiod of 12 h light and 12 h dark. *Chlorella* was adopted in this research as it is one of the dominant bloom-forming microalgae in natural waters[33] and exhibits distinctly different characteristics compared to *M. aeruginosa*.

To obtain IOM, the algal suspension was first centrifuged at 10 000 rpm for 10 min and then filtered through a 0.45 μm mixed cellulose membrane filter (Taoyuan Co. Ltd, China). The resulting algal pellet was rinsed three times using Milli-Q water (18.2 MΩ cm), resuspended, and subjected to three freeze–thaw cycles between −80 °C (ultra-low temperature freezer, Haier, China) and 35 °C (water bath, Yishan, China) over a 72 h period to induce cell lysis. Following this treatment, the suspension was centrifuged again at 10 000 rpm for 15 min, and the supernatant was filtered through a 0.45 μm cellulose membrane to obtain the IOM solution.

2.2 Experimental protocols

Potassium peroxymonosulfate ($KHSO_5$, PMS; analytical grade, >98% purity) was purchased from Aladdin Chemicals (Shanghai, China). A stock solution of PMS was prepared in advance and stored at 4 °C prior to use.

The heat-activated oxidation experiment was conducted in a temperature-controlled oxidation reactor. The PMS doses were 0.2, 0.4, 0.6, and 0.8 mM, respectively. The reaction temperature was 60 °C, and the reaction time was 60 min. After adding a certain dose of PMS into the IOM-containing feed water, a stoichiometric amount of sodium thiosulfate ($Na_2S_2O_3$; Aladdin Chemicals, Shanghai, China) was directly introduced to quench residual oxidants, with the dosage calculated on a molar basis equivalent to the added PMS. The activation temperatures (50 °C, 60 °C, 70 °C, and 80 °C) for IOM removals were also determined.

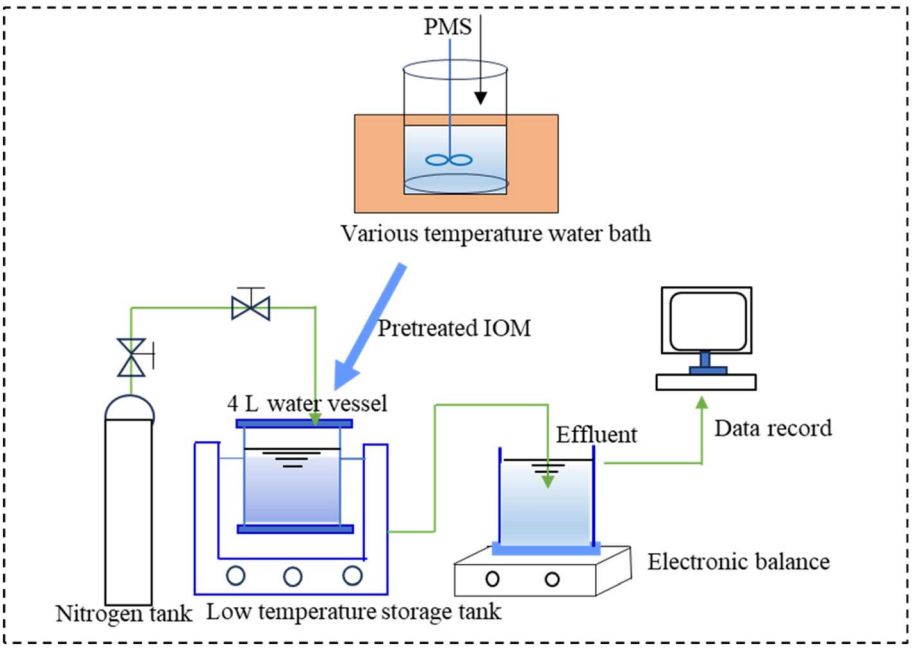

Fig. 1 Schematic of the experimental setup.

UF experiments were conducted in a dead-end filtration mode utilizing a 400 mL stirred cell (Amicon 8400, Millipore, USA), equipped with a flat-sheet polyethersulfone (PES) membrane (OM100076, Pall, USA). The schematic diagram of the experimental setup is shown in Fig. 1. The membrane had a molecular weight cut-off (MWCO) of 100 kDa and an available filtration area of 4.5×10^{-3} m^2. Before the experiments, each clean membrane was pre-soaked in Milli-Q water for a minimum of 24 h at 4 °C, followed by extensive rinsing with 5 L of Milli-Q water to eliminate residual preservatives. Filtration was conducted at an operating pressure of 0.1 MPa, and the data were recorded continuously using an electronic balance connected to a data acquisition system. To ensure reproducibility, triplicate measurements were carried out for each condition.

2.3 Analytical methods

Dissolved organic carbon (DOC) and ultraviolet absorbance (UV_{254}) were measured using a total organic carbon analyzer (TOC-VCSH, Shimadzu, Japan) and a UV/vis spectrophotometer (Hach-5000) at a wavelength of 254 nm, respectively. Fluorescence excitation-emission matrices (EEMs) were obtained using a fluorescence spectrophotometer, with excitation (E_x) and emission (E_m) wavelengths ranging from 200 to 550 nm, a scanning speed of 12 000 nm min^{-1}, and a wavelength interval of 5 nm. The maximum fluorescence intensity (FI) of the organic components was determined by Parallel Factor Analysis (PARAFAC) using the DOMFluor Toolbox in Matlab®.[34]

2.4 Assessment of fouled membranes

Surface morphology and topographical characteristics of the fouled membranes were analyzed using a scanning electron microscope (XL-30 ESEM, Philips, The Netherlands) and a multimode atomic force microscope (AFM, Nanoscope 15, Veeco, USA)s. Prior to SEM imaging, all membrane samples were dried and sputter-coated with a thin layer of gold using a precision etching and coating system (Model 682, Gatan, USA) to enhance conductivity. To identify the key functional groups in membrane foulants, Fourier transform infrared (FTIR) spectroscopy was performed on an Omnic FTIR analyzer (USA). Spectral measurements were performed over the range of 400–4000 cm^{-1} at a resolution of 4 cm^{-1} and a signal-to-noise ratio of 50 000 : 1.

The contact angles of the membrane and foulants were determined on a DCA15 contact angle and surface free energy analyzer (Germany) according to the sessile-drop method.

2.5 Interaction energy between the membrane and foulants

The short-range interaction between the membrane and foulants was evaluated by the extended Derjaguin–Landau–Verwey–Overbeek (XDLVO) theory, as described.[35] Based on the method presented by van Oss *et al.*,[36] the total interaction energy in an aqueous environment is considered as the total of three components: Lifshitz–van der Waals (LW), electrostatic (EL), and acid–base (AB) interaction energies.

$$\Delta_{fwm}^{TOT} = \Delta_{fwm}^{AB} + \Delta_{fwm}^{LW} + \Delta_{fwm}^{EL} \quad (1)$$

Here, Δ_{fwm}^{LW},Δ_{fwm}^{AB}, and Δ_{fwm}^{EL} represent the individual components of LW interfacial energy, AB interfacial energy, and EL interfacial energy, respectively. The subscripts m, w, and f are the membrane, liquid, and foulants, respectively; f, w, and m are the foulants, water, and membrane, respectively.

For the evaluation of the free energy of adhesion per unit area, Δ^{AB}, Δ^{EL}, and Δ^{LW} were obtained using the following equations,

$$\Delta G_{fi_0}^{LW} = 2\left(\sqrt{r_w^{LW}} - \sqrt{r_m^{LW}}\right)\left(\sqrt{r_f^{LW}} - \sqrt{r_w^{LW}}\right) \quad (2)$$

$$\Delta G_{h_0}^{AB} = 2\sqrt{r_{w^+}}\left(\sqrt{r_{m^-}} + \sqrt{r_{f^-}} - \sqrt{r_{w^-}}\right) + 2\sqrt{r_{w^-}}\left(\sqrt{r_m^+} + \sqrt{r_f^+} - \sqrt{r_w^+}\right) - 2\sqrt{r_m^+ r_f^-} + \sqrt{r_m^- r_f^+} \quad (3)$$

$$\Delta_{h_0}^{EL} = \frac{k\varepsilon_0\varepsilon_r}{2}\left(\xi_m{}^2 + \xi_f{}^2\right)\left[1 - \coth(kh_0) + \frac{2\xi_m\xi_f}{\xi_m{}^2 + \xi_f{}^2}\operatorname{csch}(kh_0)\right] \quad (4)$$

Here, ε_0 and ε_r denote the vacuum and relative dielectric permittivity of the solution, respectively; κ represents the inverse Debye screening length; ξ_m and ξ_f correspond to the surface potentials of the membrane and foulants, respectively, with the subscript h_0 indicating the minimum separation distance of 0.158 nm. r^{LW}, r^+, and r^- refer to the LW component, the electron acceptor, and donor parameter, respectively, which could be derived using the extended Young's equation,

$$(1 + \cos\theta)r_l^{TOT} = 2\left(\sqrt{r_s^{LW} r_l^{LW}} + \sqrt{r_s{}^+ r_l{}^-} + \sqrt{r_s{}^- r_l{}^+}\right) \quad (6)$$

$$r^{AB} = 2\sqrt{r^+ r^-} \quad (7)$$

$$r^{TOT} = r^{LW} + r^{AB} \quad (8)$$

θ is the contact angle; r^{TOT} is the total surface tension; the subscripts s and l refer to the solid surface and the liquid, respectively.

2.6 Fouling mechanism analysis

The fouling mechanism was further analyzed using classical filtration models, comprising complete blocking, standard blocking, intermediate blocking, and cake layer formation, following the method of Ho *et al.*[37] The coefficient of determination (R^2) was calculated by fitting the experimental data to each model, indicating goodness of fit.

3 Results and discussion

3.1 Effects of activation temperature on IOM removal during the heat-activated PMS treatment

Fig. 2 presents the organic content of IOM at varying PMS activation temperatures. Both DOC and UV_{254} values exhibited a progressive increase with the rising PMS activation temperature (Fig. 2a and b). Specifically, the DOC concentrations after PMS treatment were 4.794, 4.668, 5.817, and 5.520 mg L^{-1} at PMS activation temperatures of 50 °C, 60 °C, 70 °C, and 80 °C, respectively, which were 50–77.3% higher than those of IOM under control. The UV_{254} values were also 1.28–2.2 times higher than those of the control. These results suggest that heat-activated PMS pretreatment has limited efficacy in removing organics of IOM, which can be explained by the fact that PMS pretreatment might primarily oxidize large molecular organics into smaller fragments without achieving effective mineralization. This outcome sharply contrasts with previous findings for natural organic matter (NOM) and EOM, where 60 min of oxidation achieved UV_{254} and DOC removal efficiencies of 58.0% and 32.0% of NOM, respectively.[22] This discrepancy

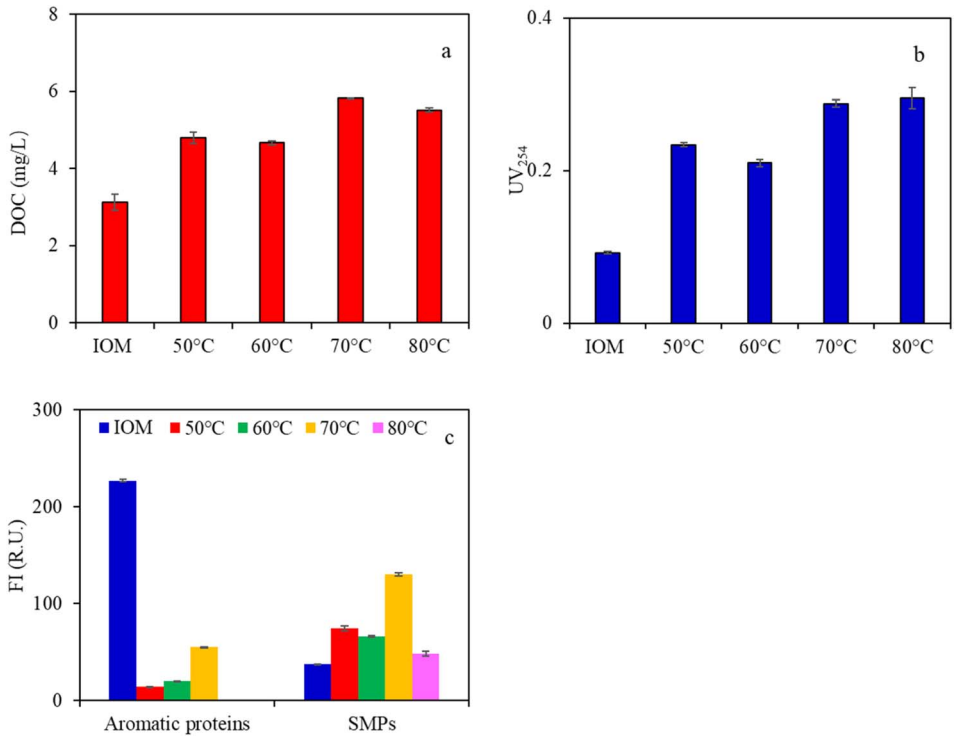

Fig. 2 Organic removal of IOM under various activation temperatures by PMS (IOM DOC = 3 mg L^{-1}, PMS = 0.4 mM, 60 min): (a) DOC content, (b) UV_{254} content, and (c) FI.

probably stemmed from the distinct structural characteristics of IOM as well as the applied PMS dose. Notably, the DOC value at 60 °C was lower than that at 70 °C and 80 °C, suggesting that PMS activation at 60 °C might induce moderate oxidation that effectively breaks down large molecular organics while minimizing the excessive generation of small molecular organics.

Analysis of the fluorescent organic components of IOM under various PMS activation temperatures (Fig. 2c) revealed two distinct fluorescent components identified among IOM across various PMS treatments by EEM-PARAFAC (Fig. S1). Component 1 (C1, E_x/E_m = 250(290)/360 nm) was attributed to aromatic protein-like substances (tyrosine), and Component 2 (C2) was associated with soluble microbial products (SMPs, tryptophan).[38] Following the heat-activated PMS treatment, the FI of C1 was significantly reduced, with 60 °C yielding the lowest FI for C1 while minimizing the excessive accumulation of SMPs. Although 80 °C resulted in the lowest FI for SMPs, considering that excessively high temperatures might induce free radical self-quenching or favor the generation of less reactive persulfate anion radicals ($SO_4^{-\bullet}$), thereby reducing the oxidation efficiency of persulfate for organic removals, 60 °C was selected as the optimal activation temperature in the following heat-activated PMS treatment.

3.2 Effectiveness of membrane fouling control by IOM through heat-activated PMS treatments

Fig. 3 depicts the filtration flux declines of IOM solutions subjected to various PMS treatments. As shown, IOM under control exhibited a pronounced decline in flux, with the final filtration flux reduced to only 20% of the initial value; in contrast, notable changes in flux behavior were observed for IOM, following the heat-activated PMS pretreatment. For instance, IOM treated with 0.2 mM PMS experienced an even more severe flux decline; however, when the PMS concentration exceeded 0.2 mM, significant improvements in filtration flux were observed, suggesting that higher PMS dosages (>0.2 mM) might effectively mitigate membrane fouling induced by IOM, while low-dose PMS may exacerbate membrane fouling. This result differs from previous studies, which can be explained by the fact that IOM predominantly comprises macromolecules, such as proteins, lipids, nucleic acids, and polysaccharides, with their molecular weights significantly higher than EOM;[39] thus, low PMS doses may be insufficient to fully oxidize these complex organics, whereas higher doses facilitate more complete oxidation. Notably, the flux observed for IOM after 0.8 mM PMS treatment was lower than that after 0.6 mM PMS pretreatment, indicating that although high PMS concentrations might effectively degrade macromolecules, thereby reducing reversible fouling, they may also generate smaller organic fragments. These fragments might contribute to increased irreversible fouling, leading to an overall variation in total fouling resistance. The above results thus indicated that heat-activated PMS oxidation can partially mitigate membrane fouling induced by IOM, especially at 0.6 mM PMS, but both insufficient and excessive PMS dosing might be unfavorable for the filtration flux improvement.

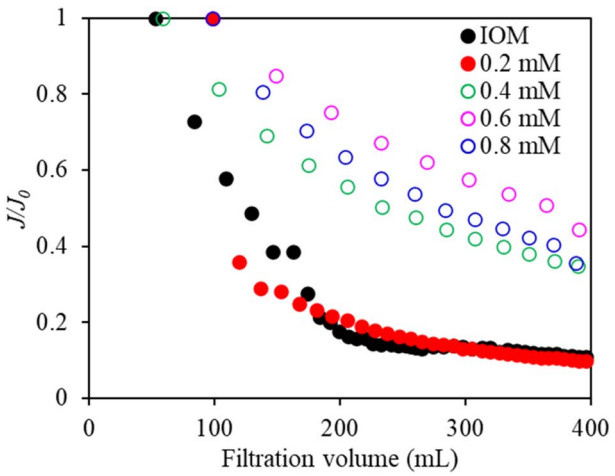

Fig. 3 Filtration flux of IOM under various PMS doses (DOC = 5 ± 0.1 mg L^{-1}, 60 °C, 60 min).

3.3 Organic characteristics and membrane foulant after various heat-activated PMS treatments

Fig. 4 shows the DOC and UV_{254} contents of IOM after various PMS treatments. PMS-treated IOM exhibited higher DOC contents compared to the control, whereas the DOC contents gradually decreased with increasing PMS dose, which suggested that higher doses of heat-activated PMS (>0.4 mM) might facilitate more thorough oxidation of organics, while lower PMS doses exhibited limited effectiveness in organic removal. This phenomenon can be explained by the fact that macromolecular organics in IOM might be oxidized into smaller substances without advancing to mineralization with PMS under low dosages of <0.4 mM; however, those organics may be further oxidized with increasing PMS dose, thus leading to the reduction of total organics (Fig. 4a). Similar trends were also observed for the UV-absorbing organics (Fig. 4b); the UV-adsorption organics were initially increased at low PMS doses, then decreased at high PMS doses >0.4 mM, suggesting that more UV-adsorption organics in IOM can also be oxidized when PMS exceeds 0.4 mM, which might be contributing to the mitigation of membrane fouling. IOM after PMS pretreatments had enhanced DOC and UV_{254} contents, whereas the filtration flux was enhanced for IOM after PMS treatments (>0.2 mM), which might be explained by the fact that the DOC content is only a measure of the total amount of dissolved organic matter that cannot provide any quantitative or qualitative information concerning its various components on membrane fouling, which was consistent with previous research.[40]

The molecular characteristics of IOM under varying PMS doses were further examined. Fig. 4c illustrates the MW distribution profiles of IOM after various heat-activated PMS treatments. The peak area rejections by PMS and UF were also analyzed using the HPSEC peak-fitting technology (Fig. 4d). As shown in Fig. 4c, the IOM solution displayed three distinct DOC response peaks: a high-MW fraction at approximately 771 000 kDa, a medium-MW fraction around 2100 kDa, and a low-MW fraction near 3500 Da. According to previous studies,[41,42] the MW fractions <1 kDa are typically associated with chlorophyll, algal toxins, odor and taste (O&T) compounds, amino acids, and

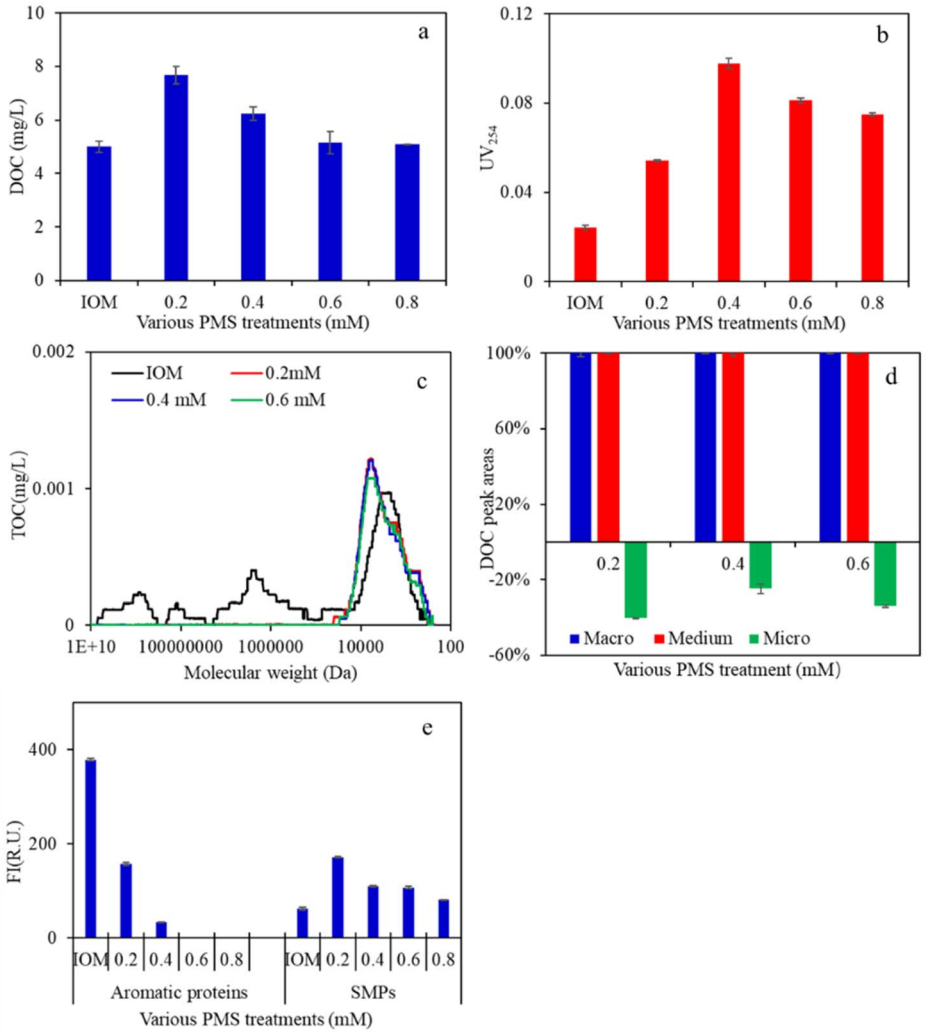

Fig. 4 Organic content, MW distribution and fluorescent organic properties of IOM by various heat-activated PMS treatments: (a) DOC content, (b) UV_{254} content, (c) MW distribution, (d) peak area rejection, and (e) FI.

other small molecules, while the components of >800 kDa and 40–100 kDa are primarily composed of macromolecular phycocyanin, carbohydrates, and medium-sized proteins/peptides, nucleic acid fragments, and certain pigment metabolites. Li *et al.* investigated the characteristics of intracellular and extracellular AOM from *M. aeruginosa* and found that 27% of the DOC in IOM was distributed in the <1 kDa range, while 42% and 31% were distributed in the 40–800 kDa and >800 kDa ranges, respectively.[39] This distribution differed markedly from that of EOM, in which the majority of organics was concentrated within the 1–100 kDa range. In the present study, the 3500 Da fraction of IOM showed significantly higher DOC peaks compared to other fractions, whereas the UV absorbance peaks of macro- and medium-MW fractions were relatively lower (Fig. S2), suggesting that macromolecular components were mainly composed of organics with weak UV absorbance. After heat-activated PMS treatment (Fig. 4d), the DOC peak areas of both macro- and medium-MW fractions were completely eliminated, with 100% reduction observed across all the PMS doses. In contrast, the low-MW fraction ranging from 200–10 kDa showed peak area reductions of −40%, −25%, and −34% for PMS doses of 0.2, 0.4, and 0.6 mM, respectively, suggesting that heat-activated PMS can efficiently degrade high- and medium-MW substances of IOM, potentially leading to the enrichment of low-MW organics of 200–10 kDa.

The fluorescent organic components of IOM under various PMS doses were also analyzed using EEM spectroscopy combined with PARAFAC. As seen (Fig. 4e), there were also two distinct fluorescent components identified across various PMS and UF treatments. IOM under control had a significantly higher FI of C1 (Fig. 4e); however, after the heat-activated PMS treatment, they were markedly reduced, especially at a PMS dose > 0.2 mM, indicating that heat-activated PMS preferentially oxidized aromatic protein-like organics of IOM. For C2 (SMPs), the FI values were 37.81, 103.41, 66.13, 64.53, and 48.47 R.U. for PMS doses of 0, 0.2, 0.4, 0.6, and 0.8 mM, respectively. This phenomenon can be explained by the fact that low doses of PMS (<0.6 mM) might lead to leakage of IOM components, such as proteins,

polysaccharides, and nucleic acid fragments, resulting in an increase in SMPs organics. However, as the PMS concentration increased, the oxidation of PMS not only enhanced the algal cell disruption but also directly oxidized the released intracellular organics, breaking them down into smaller molecules or even achieving partial mineralization. To further assess the effects of heat-activated PMS on membrane fouling control, the organic foulants and fouled membrane characteristics were examined.

Fig. 5 displays the organic removals of UF when IOM was treated after heat-activated PMS. As seen, all the DOC removal efficiencies decreased after heat-activated PMS treatments (Fig. 5a), with values of 52.9%, 48.12%, 49.12%, and 58.14% for PMS doses of 0.2, 0.4, 0.6, and 0.8 mM, respectively, which were 9.9–19.9% lower compared to direct IOM filtration. In contrast, the UV removals exhibited more variable behavior, showing efficiencies of 68.75%, 81.25%, 43.75%, and 62.5% for the corresponding PMS concentrations, compared to 43.75% of IOM under control (Fig. 5b). After heat-activated PMS treatment, UF membrane had increased rejections of UV-absorbing organics, while the DOC removal efficiency was concurrently reduced; such alterations in organic rejections might be considered as one of the explanations of enhanced filtration flux after heat-activated PMS oxidation (Fig. 3).

Peak area reductions of various molecular organics by UF were also analyzed (Fig. 5c). When IOM was filtered directly by UF, significant reductions were observed in both macro- and medium-molecular organics, with the DOC peak area decrease of 100% and 67.76%, respectively. This result aligns with previous studies, suggesting that macromolecular organics and a portion of the medium molecular fraction are the main contributors to membrane fouling.[43] Following the heat-activated PMS treatment, a significant enhancement in the rejection of low-MW organics was observed. The DOC peak area removal efficiencies of low-MW fractions were 52.41%, 15.86%, and 31.41% for PMS doses of 0.2, 0.4, and 0.6 mM, respectively, suggesting that when IOM was treated after PMS, small molecular substances in the 200–10 kDa range may evolve into significant foulants that were retained by UF, indicating a potential shift in the membrane fouling mechanism.

Analysis of fluorescent organic rejections (Fig. 5d) revealed notable changes in the rejection of fluorescent organic components, following UF. For instance, the FI removal efficiencies of C1 and C2 were 30% and 26.3% for IOM under control, respectively. In contrast, the removal efficiency changed to 91.99%, 61.0%, 0%, and 0% for C1 at PMS concentrations of 0.2, 0.4, 0.6, and 0.8 mM, respectively. For C2, the corresponding removal rates were 71.2%, 43.5%, 68.1%, and 50.11%, respectively. These findings indicated that when IOM was treated after heat-activated PMS doses, both protein-like organics and dissolved microbial products can be well rejected by UF, which further highlights the shift in dominant organic foulants, following PMS oxidation.

3.4 Characterization of fouled membrane surfaces

Fig. 6 displays the surface morphology of virgin and fouled membranes (Fig. 6a–f), and the AFM images of virgin and fouled membranes are also shown (Fig. 6a1–f1). As shown in Fig. 6b, substantial membrane fouling was observed after direct filtration of IOM, characterized by the formation of a compact cake layer and the accumulation of macromolecular organics on the membrane surface, in contrast to the clean membrane, which exhibited a smooth surface with uniformly distributed pores

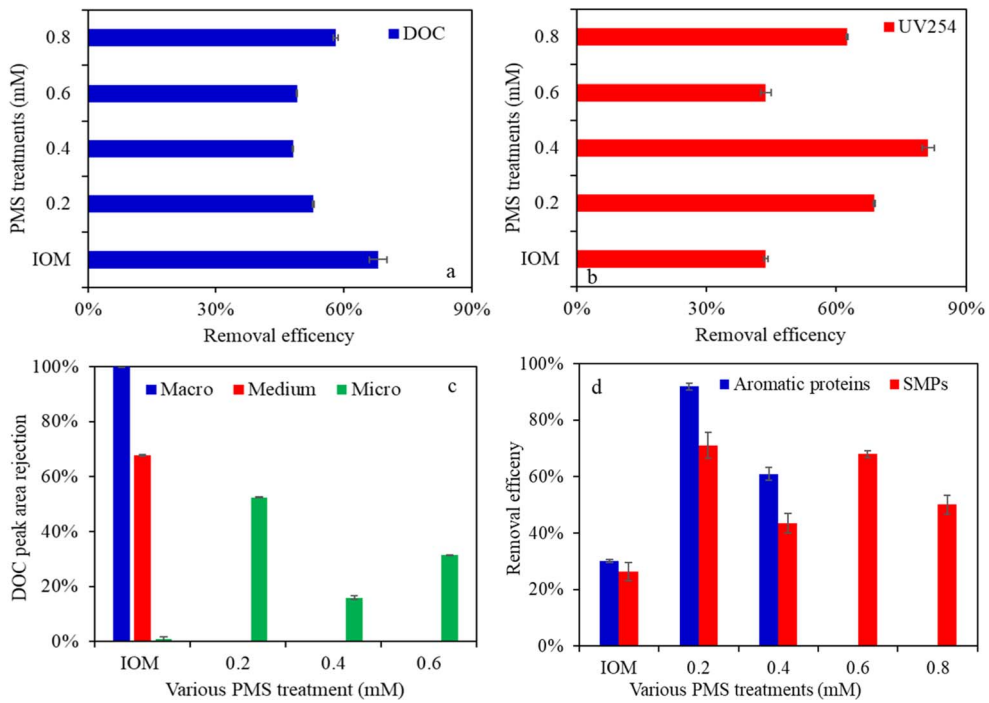

Fig. 5 Organic rejection of IOM by UF after various heat-activated PMS treatments, (a) DOC, (b) UV_{254}, (c) peak areas of molecular organics, (d) fluorescent organics.

(Fig. 6a). However, after heat-activated PMS treatment, significant changes were observed in the morphology of the fouling layer. For instance, despite several molecular organics still existing on the membrane surface, a dense cake layer was no longer clearly visible (Fig. 6d, c and f), except in the case of IOM treated with 0.2 mM PMS (Fig. 6e). In addition, the degree of connectivity and aggregation among organic substances was altered, as evidenced by the AFM images.

Fig. 6a1–f1 illustrates the surface morphologies of virgin and fouled membranes, as revealed by AFM, following different heat-activated PMS treatments. As seen, the cleaned membrane surface had relatively uniform peaks and valleys (Fig. 6a1); however, following IOM filtration, significant alterations in membrane surface roughness were observed (Fig. 6b1), *i.e.*, the mean roughness (R_a) was 9.39 for virgin membrane, and it enhanced from 36.16 to 52.20, 59.14, and 68.36 nm for IOM after 0.2, 0.4, 0.6, and 0.8 mM of PMS treatment, respectively, comparing with 33.99 of IOM under direct filtration. This result indicated that heat-activated PMS could significantly increase the membrane surface roughness, suggesting notable changes in the fouling characteristics. This behavior was markedly different from that observed for EOM fouling that the R_a was increased after heated-activated PMS, as reported by our previous research,[44] which can be explained that despite macromolecular components (proteins, polysaccharides) in IOM can be oxidized into smaller molecular organics (amino acids, short-chain carboxylic acids) after heat-activated PMS treatment, decreasing the accumulation of macro MW organics on the membrane surface and accumulation of cake layer, and the membrane fouling alleviated,[45] the metal ions (Fe^{2+}, Ca^{2+}) in algal cells might be released after heat-activated PMS oxidation, which might form metal–organic complexes with oxidized organic compounds (*e.g.*, carboxylic acids), leading the membrane rough enhanced due to the composited fouling layers on the membrane surfaces.[43]

Similar results were also observed for R_q (Table 1), the standard deviation of surface heights, which increased from 11.76 nm for the clean membrane to 50.38, 45.93, 67.26, 75.02, and 85.18 nm for membrane fouled by IOM under 0, 0.2, 0.4, 0.6, and 0.8 mM PMS dose treatments, respectively. Both SEM and AFM analyses suggested that the heat-activated PMS pretreatment markedly altered the morphology and topography of the fouling layer induced by IOM, consequently changing the antifouling performance in the UF process.

The functional groups of foulants deposited on the membrane surface were further characterized by ATR-FTIR (Fig. 7a). As shown, direct UF filtration of IOM resulted in prominent absorption bands at approximately 3350, 3224, 1653, 1405, 1071, and 1027 cm^{-1} on the fouled membrane surfaces. Prior research indicated that the broad absorbance bands peaking at 3350 and 3224 cm^{-1} were associated with O–H stretching vibrations, which are characteristics of polysaccharides.[46] The peak appearing at 1653 cm^{-1} arises from C=O stretching (amide I), indicative of peptide bonds in proteins or polypeptides.[47] The broad band around 1404 cm^{-1} is attributed to the asymmetric stretching of carboxylate groups (COO^-) or Amide III vibrations (1200–1400 cm^{-1}) in proteins.[48,49] Additionally, the peaks at approximately 1070 and

Table 1 Variation in the R_a and R_q values of fouled membranes under various PMS (mM) treatments

	Clean	IOM	0.2	0.4	0.6	0.8
R_a (nm)	9.39	33.99	36.16	52.20	59.14	68.36
R_q (nm)	11.76	50.38	45.93	67.26	75.02	85.18

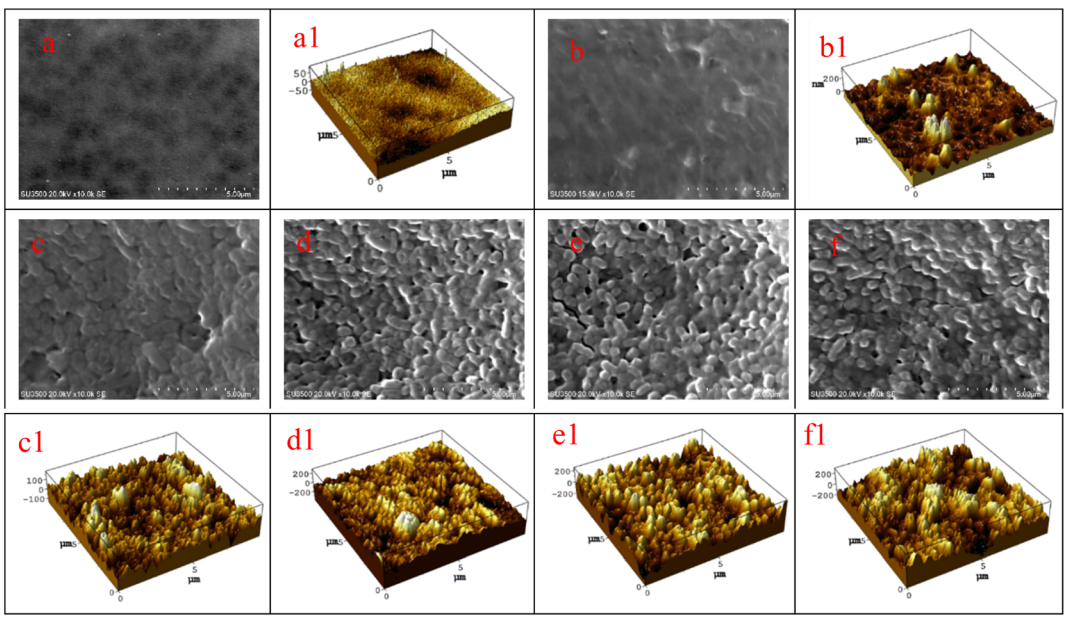

Fig. 6 SEM and AFM images of clean and fouled membranes by IOM under various PMS treatment: (a, a1) Virgin; (b, b1) IOM under control; (c, c1) PMS 0.2 mM; (d, d1) PMS 0.4 mM; (e, e1) PMS 0.6 mM; and (f, f1) PMS 0.8 mM.

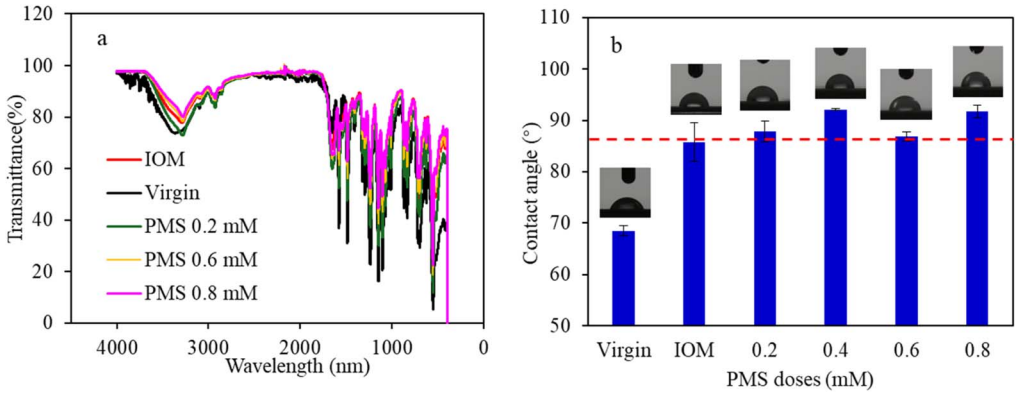

Fig. 7 Variation in functional groups (a) and contact angles (b) on the clean and fouled membrane surfaces using ATR-FTIR and contact angle measurements.

1015 cm^{-1} correspond to O–H bending and C–O or C–O–C stretching vibrations, respectively, suggesting the presence or deposition of polysaccharide-like substances. The above result indicated that the IOM-derived foulants on the membrane surface were predominantly proteinaceous and polysaccharide materials with humic components, as evidenced by MW distribution and EEM spectra (Fig. 5). After PMS treatment, the peak intensities were dramatically decreased, suggesting that polysaccharide-like and protein-like substances can be effectively removed after heat-activated PMS treatment, thereby contributing to the mitigation of membrane fouling.[50]

The contact angles of membranes fouled by IOM were also determined (Fig. 7b). As seen, the clean membrane exhibited a contact angle of 68.5°, indicating good hydrophilicity. However, after IOM direct filtration, the contact angle increased to 85.75°, which indicated a shift toward hydrophobicity. Following heat-activated PMS treatments, the contact angles were further enhanced to 87.8°, 92.08°, 86.85°, and 91.67° for IOM with PMS doses of 0.2, 0.4, 0.6, and 0.8 mM, respectively, indicating that the hydrophobicity of the fouling layer was further enhanced after heat-activated PMS treatment. This phenomenon can be explained by the fact that PMS oxidation may break down macromolecular organics in IOM, leading to the formation of smaller, more hydrophobic organic compounds, such as aromatic compounds and/or nitrogen-containing heterocyclic molecules. These oxidation products, being highly hydrophobic, might tend to accumulate on the membrane surface, thereby contributing to the generation of a hydrophobic fouling layer. However, the total content of macromolecular organics that induced membrane fouling was reduced after PMS treatment, alleviating membrane fouling. Guo *et al.*[22] investigated the application of heat-activated peroxydisulfate pre-oxidation for degrading contaminants and mitigating UF membrane fouling in natural surface water treatment and found that| after PDS oxidation, the contact angle of the membrane fouled by pretreated water was higher than that of the membrane fouled by feed water, which might be due to the reduction of the amount of contaminants in the water as well as the variation of the characteristics of organic foulants.

3.5 Variation in the interaction energy between the membrane and foulants

The surface tension parameters and membrane–foulant interaction energies were also quantitatively analyzed to further assess the efficacy of heat-activated PMS treatment in membrane fouling mitigation. As shown (Table 2), most organic foulants, following heat-activated PMS treatments, demonstrated significantly elevated electron donor components (γ^-) compared to untreated IOM, likely attributable to the oxidative generation of carboxylate groups on foulant molecules.[51,52] In addition, the r^{AB} increased for IOM treated with heat-activated PMS relative to the control, implying enhanced chemical bond interactions among organic molecules.

Regarding the Δ_{fmf}^{co} among organic foulants, all the foulants displayed negative values both with and without the PMS

Table 2 Δ_{fsf}^{co} (mJ m^{-2}) of organic foulants by various heat-activated PMS (mM) treatments

	r^{Lw}	r^+	r^-	r^{AB}	r^{TOT}	Δ_{fmf}^{LW}	Δ_{fmf}^{AB}	Δ_{fmf}^{co}
Virgin	0.011	17.26	294.27	142.54	142.55	−41.69	43.34	
IOM	39.13	0.003	8.71	0.30	39.42	−5.03	−41.95	−46.98
0.2	48.61	8.92	118.69	65.08	113.70	−10.61	48.23	37.62
0.4	1.24	10.48	1.19	7.07	8.31	−25.28	−28.68	−53.96
0.6	48.62	37.94	101.93	124.37	172.99	−10.62	−22.40	−33.02
0.8	0.044	15.88	9.46	24.52	24.56	−39.77	−8.41	−48.18

Table 3 Δ_{fsm}^{Ad} (mJ m^{-2}) of membrane and foulants by various heat-activated PMS (mM) treatments

	Δ_{fwm}^{LW}	Δ_{fwm}^{AB}	Δ_{fwm}^{AD}
IOM	−5.67	−33.28	−38.94
0.2	−9.03	−8.32	−17.35
0.4	12.70	−43.69	−30.99
0.6	−8.23	52.70	44.48
0.8	15.92	−22.19	−6.27

treatment. While the Δ_{fmf}^{co} was less negative for IOM treated with 0.6 mM PMS compared to other treatments. Δ_{fmf}^{co} quantifies the free interaction energy between identical material surfaces in aqueous contact, serving as a thermodynamic metric for membrane/colloid hydrophobicity. A negative Δ_{fmf}^{co} signifies a thermodynamically unstable state (hydrophobic surfaces) and favorable foulant–foulant adhesion, whereas a positive value suggests a stable state (hydrophilic surfaces), with spontaneous foulant repulsion. The above results suggested that although all the foulants (except those from IOM treated with 0.2 mM PMS) exhibited thermodynamic instability (negative Δ_{fmf}^{co}), the foulants formed after 0.6 mM PMS treatment were comparatively more hydrophilic than those from other treatments. The oxidation induced by 0.6 mM PMS might also have superior hydrophilicity transformation efficiency, leading to a greater reduction of fouling potential. IOM subjected to various heat-activated PMS treatments exhibited enhanced attractive cohesion interaction energy relative to the control. This phenomenon might be explained by the formation of highly reactive radicals ($SO_4^{\bullet-}$ and $^{\bullet}OH$) during PMS oxidation, which degrade organics in IOM, such as polysaccharides, proteins, and lipids, into smaller compounds (*e.g.*, organic acids, aldehydes, and ketones). Concurrently, polar functional groups, including carboxyl, hydroxyl, and aldehyde groups, might be introduced, increasing oxygen-containing moieties that enhance intermolecular interactions, such as hydrogen bonding and/or van der Waals forces (Table 2). Possible polymerization or cross-linking reactions might also occur among organic molecules, resulting in enhanced molecular binding and aggregation stability.[50,53,54]

Analysis of the free energy of adhesion (Δ_{fwm}^{AD}) revealed that acid–base interactions between the membrane and foulants also exerted significant effects during the initial formation of membrane fouling; however, these interactions changed considerably between the membrane and foulants after various PMS treatments. As shown in Table 3, all the Δ_{fwm}^{AD} values were negative, except for the IOM treated with 0.6 mM PMS. Besides, they were negatively reduced with increasing with PMS dose. For instance, the Δ_{fwm}^{AD} was −38.94 for IOM under control, while it changed to −17.35, −30.99, and −6.27 for IOM treated with PMS 0.2, 0.4, and 0.8 mM, respectively. Prior research indicated that Δ_{fwm}^{AD} is correlated with the decline in the primary filtration flux.[55] A negative Δ_{fwm}^{AD} value indicates attractive interactions between the membrane and foulants, promoting fouling, while a positive value suggests repulsion instead. The results suggested that for IOM, following heat-activated treatment with PMS doses of 0.2, 0.4, and 0.8 mM, the organics were more likely to be adsorbed onto or into the membrane due to attractive adhesion energy, leading to potential fouling. In contrast, after

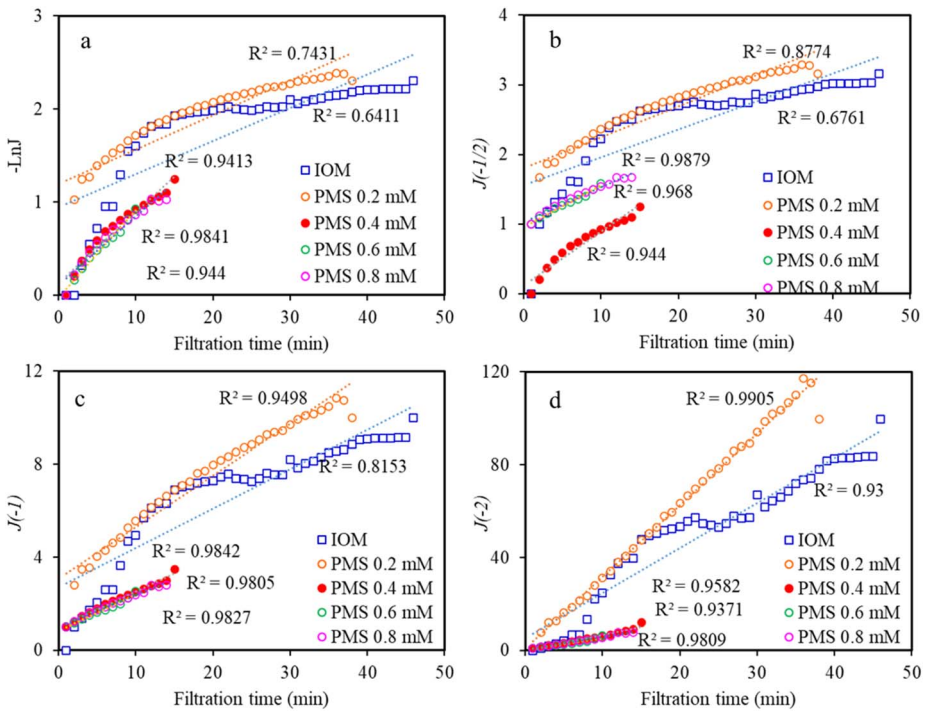

Fig. 8 Regression analyses of IOM fouling under various PMS treatments: (a) complete blocking, (b) standard blocking, (c) intermediate blocking, and (d) cake layer formation.

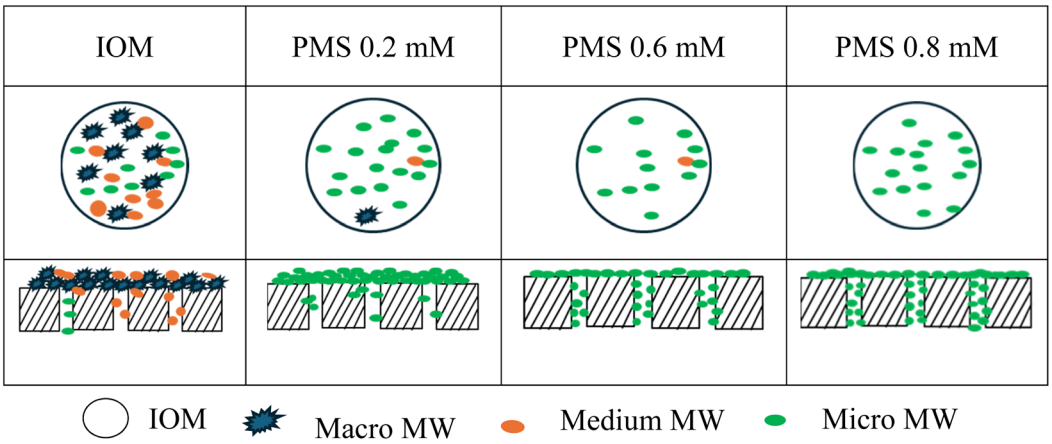

Fig. 9 Fouling mechanism of the membrane induced by IOM after various heat-activated PMS treatments.

pretreatment with 0.6 mM PMS, the repulsive interaction between the membrane and foulants likely hindered their deposition and penetration into membrane pores, thereby alleviating initial flux decline. The reduced attractive or even repulsive Δ_{fwm}^{AD} between the membrane and foulants observed after PMS treatment than IOM under control may be considered as one of the explanations for the alleviated membrane fouling.

Both the Δ_{fwm}^{AD} and Δ_{fmf}^{co} further indicated that the heat-activated PMS treatment significantly affected the adhesion interaction energy between the membrane and foulants, as well as the cohesion interaction energy between organic foulants and foulants during the UF of IOM, potentially contributing to the variation of membrane fouling.

3.6 Membrane fouling mechanisms

To further investigate the effects of heat-activated PMS treatments on IOM membrane fouling mechanisms, the experimental data were fitted by employing four well-established filtration models (Fig. 8). The R^2 followed the order of cake layer formation (0.9257) > intermediate blocking (0.8175) > standard blocking (0.732) > complete blocking (0.6317) for untreated IOM (control), suggesting that cake layer formation dominated the fouling process during the IOM direct UF filtration. However, after heat-activated PMS pretreatment, the fouling mechanism was significantly changed, with intermediate blocking exhibiting the highest R^2 values. Further analysis of the fouling rate constants ($\propto_b$, $\propto_p$, $\propto_s$, $\propto_c$) suggested that all samples exhibited the following trend of $\propto_c > \propto_s > \propto_p > \propto_b$ regardless of PMS dosage (Table S1, in the SI). Notably, the increasing PMS dosage led to progressive enhancement of complete blocking ($\propto_b$) and standard blocking ($\propto_p$) rate constants; for instance, the $\propto_b$ increased from 0.0371 (PMS 0.2 mM) to 0.0945 (PMS 0.6 mM), while for $\propto_p$, it showed a similar increasing trend from 0.0443 to 0.0603. Conversely, the rate constants for intermediate blocking ($\propto_s$) and cake layer formation ($\propto_c$) displayed a decreasing trend with PMS dosage, showing reductions of 3.9–14.8% and 64.4–71.4%, respectively, compared to those of IOM under control (except at 0.2 mM PMS). These findings suggest that PMS oxidation might effectively mitigate membrane fouling, stemming from cake layer formation and intermediate blocking; however, it may concurrently aggravate fouling associated with complete and standard blocking, indicating a transformation in fouling behavior induced by heat-activated PMS oxidation during IOM filtration.

The contributing factors (CF) of various rate constants were also assessed to elucidate their roles in membrane fouling (Fig. S3). As shown, cake layer formation ($\propto_c$) dominated the fouling process in untreated IOM, accounting for approximately 89.29% of the total fouling resistance, which aligns with the findings presented in Table S1. Meanwhile, following PMS pretreatment, the CF of $\propto_c$ decreased significantly, showing 18.84–25.85% ($p < 0.05$) reduction compared to the control, indicating effective mitigation of cake layer formation. This reduction was likely due to the oxidative breakdown of macro-MW substances by PMS, which reduces the propensity of these compounds to accumulate on the membrane surface. By comparison, the contributions of intermediate blocking ($\propto_s$), complete blocking ($\propto_b$), and standard blocking ($\propto_p$) increased with PMS dosage. Specifically, the CF of $\propto_s$ increased from 7.54% to 16.07%, 18.33%, and 17.05% at PMS doses of 0.4, 0.6, and 0.8 mM, respectively, which was an 8.52–10.78% increase over the control. Meanwhile, the CFs of $\propto_b$ and $\propto_p$, increased by approximately 4.18–6.31 fold and 2.4–3.3 fold, respectively, relative to the IOM under control, which revealed a distinct shift in the dominant fouling mechanism from cake formation to pore-blocking after PMS treatment. Based on the above analysis, the fouling mechanism by PMS treatment was proposed, as shown in Fig. 9.

Collectively, these findings highlight the efficacy of heat-activated PMS as a pretreatment for controlling membrane fouling in algae-laden water treatment, particularly by targeting the IOM release during algal late growth phases or under external stressors (*e.g.*, oxidative damage, hydraulic shear), which provides a promising strategy for optimizing UF performance in complicated water environments.

4 Conclusions

This study explored the control and fouling mechanisms of UF caused by IOM through heat-activated peroxydisulfate pre-oxidation. The key findings are summarized as follows:

(1) Heat-activated PMS effectively mitigated the membrane fouling induced by IOM, especially at PMS dosages of >0.2 mM, with the optimal performance at PMS 0.6 mM. Macro and medium MW organics of proteins, polysaccharides, as well as humic-like organics, were the primary membrane foulants during UF. Following heat-activated PMS pre-oxidation, these organics were well oxidized. Furthermore, the fluorescent aromatic protein-like organics within IOM were effectively eliminated, as confirmed by fluorescence spectroscopy.

(2) Analysis of the interaction energy between the membrane and foulants suggested that although the PMS-treated IOM exhibited moderately enhanced cohesive attractive interactions relative to the control, the organics formed after 0.6 mM PMS treatment displayed superior hydrophilicity compared to those subjected to other PMS dosages. Furthermore, the adhesive interaction energy between the membrane and foulants was either attractively reduced or reversed from attractive to repulsive, thereby mitigating membrane fouling. The surface morphology and hydrophobicity of the fouling layer were also changed after PMS pretreatment.

(3) Cake layer formation was the major fouling mechanism when untreated IOM was filtrated by UF, whereas the fouling mechanism was switched from cake layer formation to pore blocking after heat-activated PMS treatment. This study proposed a practical strategy for mitigating IOM-induced membrane fouling in the UF of algal-laden water.

Author contributions

Weiwei Huang: conceptualization, performed all the experiments and wrote the main manuscript text; Weiwei Lv: data analysis; Quan Yuan: data analysis; Hang Yang: methodology; Yuning Zhang: investigation; Wenzong Zhou: review, editing and funding acquisition.

Conflicts of interest

The authors declare that there are no competing financial or personal interests that could have influenced the work reported in this work.

Data availability

The authors declare that the data supporting the findings of this study are included within the article.

Acknowledgements

This research was finally supported by Shanghai Agricultural Science and Technology Innovation Project, China (V2024002), the China Agriculture Research System of MOF and MARA (CARS-46), and the Outstanding team of Shanghai Academy of Agricultural Sciences (2025-031).

References

1 X. Yang, L. Yao, Y. Wang, X. Zhang and P. Ren, *Chem.–Eng. J.*, 2022, **445**, 136689.
2 X. Cheng, J. Lian, Z. Ren, C. Hou, Y. Jin, L. Zhang, X. Zhu, C. Luo, D. Wu and H. Liang, *Water Res.*, 2021, **204**, 117622.
3 W. L. Yang, F. Zhou, J. Lee, J. Kim, D. Y. Kwon, Y. Kim, H. Q. Ren, S. K. Hong, M. Zhan and B. Wu, *J. Cleaner Prod.*, 2024, **479**, 144084.
4 Z. M. Wang, S. Zhang, L. L. Li, X. M. Zang, R. Zulekha, H. Y. Zhang and X. Z. Zhang, *Sep. Purif. Technol.*, 2025, **350**, 124567.
5 D. Y. Kwon, D. H. Kwon, J. Lee, J. Lim and S. Hong, *Desalination*, 2025, **600**, 118505.
6 Y. Y. Wang, M. N. Li and H. Yang, *Sep. Purif. Technol.*, 2025, **364**, 132370.
7 K. Y. Tian, X. X. Xu, J. F. Zhu, S. T. Cao, Z. L. Yin, F. L. Li and W. B. Yang, *J. Environ. Chem. Eng.*, 2024, **12**(6), 114718.
8 F. S. Qu, Z. M. Yang, X. L. Li, R. H. Yu, Z. H. Pan, G. D. Fan, J. G. He and H. W. Rong, *Sep. Purif. Technol.*, 2021, **257**, 117877.
9 Z. J. Ren, S. Y. Wang, Q. W. Wang, L. Y. Lv, D. Y. Xu, Y. L. Dong, J. L. Han, M. Ulbricht, L. Sun and X. Y. Liu, *Sep. Purif. Technol.*, 2023, **314**, 123612.
10 H. Lee, J. Lim, M. Zhan and S. Hong, *Desalination*, 2019, **467**, 219–228.
11 F. Chen, G. Huang, F. Yao, Q. Yang, Y. Zheng, Q. Zhao and H. Yu, *Water Res.*, 2020, **173**, 115559.
12 Y. Wan, P. C. Xie, Z. P. Wang, J. W. Ding, J. Q. Wang, S. L. Wang and M. R. Wiesner, *Water Res.*, 2019, **158**, 213–226.
13 B. Liu, F. S. Qu, H. R. Yu, J. Y. Tian, W. Chen, H. Liang, G. B. Li and B. Van der Bruggen, *Environ. Sci. Technol.*, 2018, **52**(2), 765–774.
14 X. X. Cheng, D. J. Wu, H. Liang, X. W. Zhu, X. B. Tang, Z. D. Gan, J. J. Xing, X. S. Luo and G. B. Li, *Water Res.*, 2018, **145**, 39–49.
15 H. S. Zheng, Y. J. Zheng, L. Yuan, S. Li, J. F. Niu, X. Dong, Y. K. Leong, D. J. Lee and J. S. Chang, *Bio. Technol.*, 2024, **402**, 130806.
16 L. Yun, Z. Gao, X. Cheng, P. Li, L. Wang, N. Guo, C. Luo, X. Zhu, B. Liu, D. Wu and H. Liang, *Chemosphere*, 2022, **303**, 135037.
17 B. X. Ji, M. B. Asif and Z. H. Zhang, *Sep. Purif. Technol.*, 2023, **309**, 123043.
18 B. X. Ji, Y. Li and Z. H. Zhang, *Sep. Purif. Technol.*, 2023, **322**, 124308.
19 N. Li, S. Wu, H. Dai, Z. J. Cheng, W. C. Peng, B. B. Yan, G. Y. Chen, S. B. Wang and X. G. Duan, *Chem.–Eng. J.*, 2022, **450**, 137976.
20 I. A. Ike, J. D. Orbell, M. Duke and A. C. S. Sus, *Chem. Eng.*, 2018, **6**, 4345–4353.
21 Y. E. Kim, Y. Y. Ahn, M. J. Kim, J. Choi, D. Min, J. Kim, G. H. Moon and J. Lee, *Chem.–Eng. J.*, 2023, **478**, 147472.

22 Y. Guo, H. Liang, L. Bai, K. Huang, B. Xie, D. Xu, J. Wang, G. Li and X. Tang, *Water Res.*, 2020, **179**, 115905.
23 M. B. Asif, B. X. Ji, T. Maqbool and Z. H. Zhang, *Desalination*, 2021, **516**, 115225.
24 R. G. Wang, T. C. Wang, G. Z. Qu, Y. Zhang, X. T. Guo, H. Z. Jia and L. Y. Zhu, *Water Res.*, 2021, **196**, 117027.
25 S. Z. Nie, Q. Wang, Y. Liao, J. Z. Zhang, F. Yang, S. H. Wang, M. Yang and J. W. Yu, *Sep. Purif. Technol.*, 2023, **320**, 124206.
26 Z. W. Zhou, J. K. Yan, X. Li, J. W. Ren, H. Liang and Y. W. Liu, *J. Membr. Sci.*, 2024, **693**, 122353.
27 B. Liu, F. S. Qu, H. Liang, Z. D. Gan, H. R. Yu, G. B. Li and B. Van der Bruggen, *J. Membr. Sci.*, 2017, **528**, 178–186.
28 H. Yang, L. Li, J. Y. Li, S. L. Yu, N. Y. Gao and C. F. Togbah, *Sep. Purif. Technol.*, 2024, **334**, 126030.
29 X. B. Tang, T. C. Guo, H. Q. Chang, X. Yue, J. L. Wang, H. K. Yu, B. H. Xie, X. W. Zhu, G. B. Li and H. Liang, *Engineering*, 2022, **19**, 40–49.
30 C. J. Liu, Z. W. Zhou, X. Li, R. Yu, H. Q. Chang, J. W. Ren and C. Y. Wang, *J. Membr. Sci.*, 2023, **680**, 121757.
31 J. L. Han, L. Sun, Z. J. Ren, Z. Y. Chen, J. Ma and C. X. Yang, *Chem.–Eng. J.*, 2025, **467**, 147797.
32 Y. T. Zhao, Z. W. Zhou, C. J. Liu, X. Li, T. Y. Wang and F. S. Qu, *J. Membr. Sci.*, 2025, **717**, 123613.
33 Y. W. Zhang, G. Q. Liu, Y. Yang, D. L. Lu, L. F. Liu, Y. F. Wei, N. Sun and Y. Su, *Mar. Environ. Res.*, 2023, **184**, 105855.
34 C. A. Stedmon and R. Bro, *Limnol. Oceanogr.:Methods*, 2008, **6**, 572–579.
35 M. Elimelech, J. Gregory, X. Jia and R. Williams, *Particle Deposition and Aggregation: Measurement, Modelling and Simulation*, Oxford, England, 1995.
36 C. J. van Oss, *Interfacial Forces in Aqueous Media*, Marcel Dekker Inc., New York, 1994.
37 C. C. Ho and A. L. Zydney, *J. Colloid Interface Sci.*, 2000, **232**, 389–399.
38 S. K. L. Ishii and T. H. Boyer, *Environ. Sci. Technol.*, 2012, **46**, 2006–2017.
39 L. Li, N. Gao, Y. Deng, J. Yao and K. Zhang, *Water Res.*, 2012, **46**, 1233–1240.
40 J. X. Liu, Z. H. Wang, B. Z. Dong and D. S. Zhao, *Colloids Surf., A*, 2016, **511**, 320–328.
41 R. K. Henderson, A. Baker, S. A. Parsons and B. Jefferson, *Water Res.*, 2008, **42**(13), 3435–3445.
42 R. K. Henderson, S. A. Parsons and B. Jefferson, *Water Res.*, 2010, **44**(12), 3617–3624.
43 S. Zhou, Y. Zhang, J. Li, *et al.*, *J. Membr. Sci.*, 2021, **618**, 118682.
44 W. W. Huang, W. G. Lv, T. Li, H. Yang, Q. Yuan, W. Zhou and J. X. Liu, *Environ. Res.*, 2024, **263**, 119986.
45 Y. Zhang, W. D. Kang, H. T. Yu, S. Chen and X. Quan, *J. Hazard. Mater.*, 2020, **398**, 122879.
46 J. Y. Tian, C. W. Wu, H. R. Yu, S. S. Gao, G. B. Li, F. Y. Cui and F. S. Qu, *Water Res.*, 2018, **132**, 190–199.
47 X. Song, W. Luo, J. McDonald, S. Khan, F. Hai, W. Price and L. Nghiem, *Sci. Total Environ.*, 2018, **628–629**, 358–365.
48 A. Barth, *Bioenergetics*, 2007, **1767**, 1073–1101.
49 L. Sun, Y. Tian, H. Li and Q. Wang, *Environ. Intern.*, 2021, **151**, 106439.
50 B. Wang, Y. Zhang, Y. Y. Qin and H. J. Li, *Chem.–Eng. J.*, 2021, **403**, 126381.
51 W. Fu, Y. Zhou, H. Yang, H. Guo, C. Y. Tang, B. Liu, J. Liu and W. Huang, *J. Membr. Sci.*, 2025, **723**, 123930.
52 J. X. Liu, Z. H. Wang, C. Y. Tang and J. O. Leckie, *Environ. Sci. Technol.*, 2018, **52**(6), 1471–1478.
53 Y. L. Zhao, X. Z. Yuan, X. D. Li, L. B. Jiang and H. Wang, *J. Hazard. Mater.*, 2021, **409**, 124893.
54 J. L. Wang and S. Z. Wang, *Chem.–Eng. J.*, 2018, **334**, 1502–1517.
55 Q. Li and M. Elimelech, *Environ. Sci. Technol.*, 2004, **38**, 4683–4693.